Journal of Power Sources 182 (2008) 52–60

Contents lists available at ScienceDirect

Journal of Power Sources

journal homepage: www.elsevier.com/locate/jpowsour

Cobalt molybdenum carbides as anode electrocatalyst for proton exchange membrane fuel cell

Shamsul Izhar, Masatoshi Nagai*

Graduate School of Bio-applications and Systems Engineering, Tokyo University of Agriculture and Technology, 2-24 Nakamachi, Koganei, Tokyo 184-8588, Japan

ARTICLE INFO

Article history:
Received 19 October 2007
Received in revised form 18 March 2008
Accepted 22 March 2008
Available online 10 April 2008

Keywords:
Co-Mo carbide
Anode electrocatalyst
PEM fuel cell
XRD
XPS
TPR

ABSTRACT

Cobalt molybdenum (Co-Mo) carbides were prepared by the carburization of Co-Mo oxides at temperatures of 723–973 K in a stream of CH_4/H_2 gas. The carburized catalysts were evaluated using a single-stack fuel cell and three-electrode cell. The results showed high activities for the anodic electrooxidation of hydrogen over the Co-Mo catalysts carburized at 873 and 923 K. The 873 K carburized Co-Mo catalyst had the highest activity and achieved 10.9% of the performance of a commercial Pt/C catalyst in a single-stack fuel cell. The XRD, TPC, TPR and XPS results showed that the Co-Mo oxycarbide in the bulk and on the surface are the active species for the hydrogen oxidation reaction.

1. Introduction

Fuel cells have been highly considered as an alternative power source for the near future. Among the fuel cells that are currently used today are the low temperature-operated proton exchange membrane fuel cells (PEMFC), which have gained interest for use in automotive and stationary applications. Since the current PEMFC is made of electrode assemblies consisting of Pt-metal alloy electrocatalysts, the cost to produce and commercialize fuel cells is high [1,2]. Therefore, the major challenges in fuel cell research are to reduce the cost of the electrocatalyst either by lowering the Pt loading or by developing a non-noble catalyst.

Since transition metal carbides, typically of group 6, have been reported to have Pt-like chemical reactivities and electronic properties [3–8], there have been many studies related to the development of transition metal carbides for use as hydrogen fuel cell electrocatalysts [9]. For instance, tungsten carbide [10,11] and molybdenum carbide [12–14] have been the most studied. For the bimetallic carbide, a study showed that Ta-WC enhances the electrocatalytic activity due to its resistance towards corrosion [15] while other investigators have revealed the high hydrogen and methanol oxidation activities over carburized Mo-W [16,17], Ni-Mo [18] and Ni-W [19] due to the high exchange current density. The Ni-W and Ni-Mo carbides have also been studied as electrocatalysts for fuel cell anodes, taking advantage of their tolerance towards sulfur poisoning and coke formation [20].

Among all the studied transition metal carbides, cobalt molybdenum carbide has not been investigated as an anode electrocatalyst although it exhibited a high activity for the water gas-shift reaction [21], hydrotreatment reaction [22,23] and for the decomposition of methane [24]. In this study, Mo was incorporated with Co to form a bimetallic oxide. The Co-Mo oxides were then carburized in 20 wt% CH_4/H_2 at various temperatures between 723 and 973 K and supported on Ketjen carbon (KC). The catalysts were evaluated in a single-stack fuel cell and the electrooxidation of hydrogen was studied by voltammetric methods. X-ray diffraction (XRD), temperature programmed carburization (TPC), temperature programmed reduction (TPR) and X-ray photoemission spectroscopy (XPS) were used to characterize the catalysts for the determination of the active carbide species for hydrogen oxidation in a single-stack fuel cell.

2. Experimental

2.1. Preparation of catalyst and MEA

The oxidic precursors of the Co-Mo carbides were prepared by the co-precipitation of a mixture of aqueous solutions of

* Corresponding author. Tel.: +81 423 88 7060; fax: +81 423 88 7060.
E-mail address: mnagai@cc.tuat.ac.jp (M. Nagai).

0378-7753/$ – see front matter © 2008 Elsevier B.V. All rights reserved.
doi:10.1016/j.jpowsour.2008.03.084

8.5 mmol cobalt nitrate 6-hydrate ($Co(NO_3)_2{\cdot}6H_2O$, Kishida Chemical Co., 99%) and 2.8 mmol ammonium heptamolybdate 4-hydrate ($(NH_4)_6Mo_7O_{24}{\cdot}4H_2O$, Kishida Chemical Co., 99%). The solid hydroxide products were dissolved in water at 353 K while being stirred, dried overnight at 373 K, and then heated at 773 K for 5 h to obtain $CoMoO_4$ that was confirmed by XRD. A 0.2 g sample of the $CoMoO_4$ was placed on a porous quartz plate in a microreactor (10 mm i.d.), calcinated in dry air, oxidized at 773 K for 1 h, and then cooled to 573 K. The oxidized catalyst was carburized from 723–973 K at the rate of 1 K min^{-1} with 20% CH_4/H_2 (99.999%), and maintained at its final temperature for 2 h. The carburizing product was then cooled to room temperature and passivated overnight in a stream of 1% O_2/He. Ketjen carbon (Cabot Co.) was then mixed with the Co-Mo carbides in methanol so that the concentration of the catalyst was 30 wt% followed by drying overnight in air. These KC supported Co-Mo catalysts were placed in the anode and a 20 wt% Pt/C (EC-20-PTC, ElectroChem, Inc.) was used in the cathode of all the fuel cells. The 20 wt% Pt/C was also used as the anode catalyst for comparison of the Co-Mo carbide activity. For the sake of simplicity, CoMoC-873/KC was denoted as the Co-Mo catalyst carburized at 873 K and supported on KC.

The membrane electrode assembly (MEA) was prepared in-house by a common method [25] and is briefly described as follows. A membrane sheet (Nafion 117; Du Pont Co.) was boiled in an aqueous solution of 3 wt% H_2O_2, followed by deionized water and then 0.5 M H_2SO_4, all carried out at 363 K. Each step took approximately 1 h. The boiled membrane was dried overnight at 363 K and then under vacuum for 1 h prior to use. The catalyst ink was prepared by the addition of ethanol to the catalyst in a 20:1 ratio. An aqueous solution of 5 wt% Nafion (Aldrich) was directly added to the catalyst/ethanol slurry to obtain a 3.3 wt% catalyst content, and then stirred in an ultrasonic mixer. The CoMoC/KC and 20 wt% Pt/C were directly sprayed onto both sides of a membrane sheet at 333 K using an airbrush gun to produce a catalyst loading of 1 mg cm^{-2}. Two sheets of carbon cloths (Toray Co.) were placed on the outside of the sprayed anode and cathode layers followed by hot pressing, which was performed at an 11 MPa gauge pressure and 403 K for 5 min.

2.2. Electrochemical activity measurement

The polarization curves were assessed using a 5 cm^2 single-stack fuel cell (ElectroChem Co.) in flowing humidified hydrogen and oxygen in order to evaluate the activity of the catalyst versus Pt/C. The oxygen and hydrogen gasses were bubbled in water at 353 K and at a constant flow rate of 60 mL min^{-1}. The fuel cell anode and cathode was at a constant 338 K and without any back pressure. The anode and the cathode gas line temperatures were always 20 K above the cell temperature to ensure no water condensation in the gas lines. The current density at a fixed potential ($I_{0.7V}$) was evaluated instead of the short circuit current in the fuel cell as this is less susceptible to errors associated with transport losses, and closer to an actual application. All the *I–V* curves were collected on the basis of the assumption that the cathode polarization was the same for the purpose of comparison among the anodes. A two-electrode cell analysis was performed in the single-stack fuel cell using the same configuration as in the *I–V* measurement. Instead of O_2, a hydrogen-fed cathode was used as both the reference and counter electrodes, while the anode fed with hydrogen served as the working electrode.

Slow scan voltammetry (SSV) was performed on a dual compartment three-electrode cell equipped with a rotating disk electrode (Hokuto Denko Co.). A glassy carbon disk was used as the working electrode, a platinum wire as the counter electrode and a standard calomel electrode as the reference electrode. A 20 μg sample of the catalyst was spread onto the glassy carbon using a micropipette. The measurement was carried out in 0.5 M H_2SO_4 at room temperature while rotating at 2000 rpm. The exchange current density (j_0) was determined by the linearized Butler-Volmer rate law, $j = j_0 nf\eta$ (where $f = F/RT$), assuming a charge transfer kinetic limited at low potential deviation from equilibrium. The carburized catalysts were tested for passivity in 0.5 M H_2SO_4, an environment almost similar in a PEFC. A constant potential of 0.24 V (RHE) was applied to the working electrodes while the current density was measured at room temperature.

2.3. Characterization

The bulk structure of the catalyst was measured by XRD (30 kV, 28 mA). The diffraction pattern was obtained using a RINT2000 (Rigaku Co.) with Cu Kα radiation (λ = 1.542 Å). The XRD spectra were identified as $CoMoO_4$ (JCPDS #21-868, 25-1434), CoO (43-100), Co_3O_4 (42-1467), MoO_3 (09-209), MoO_2 (32-671), β-Mo_2C (31-871), η-Mo_3C_2 (42-890) and Co metal (15-806). The peaks of the Co-Mo oxycarbide and Co-Mo carbide were identified by the broad peaks of $2\theta = 37.5^\circ$ and 42.5° [24], and $2\theta = 37.0^\circ$, 43.0° and 63.1° [22], respectively. The specific surface area of the catalyst (0.1 g) was measured using an Omnisorp 100CX (Beckman Coulter Co.) at liquid nitrogen temperature after the catalyst was evacuated at 473 K for 2 h. TPC was performed to obtain the desorbed products in the gas phase that was analyzed using a quadrupole mass spectrometer (Quastar 422, Balzers Co.). Methane ($m/z = 15$) and the desorbed gases of CO ($m/z = 28$) and H_2O ($m/z = 18$) were qualitatively analyzed using the quadrupole mass spectrometer at a scan speed of 10 scan s^{-1} during the TPC. TPR was carried out to obtain the degree of reduction of the carburized catalyst using a stream of H_2 at the flow rate of 0.9 L h^{-1}. The evolution of H_2O and methane gas during the TPR was quantitatively measured using the quadrupole mass spectrometer. The spectrum of CH_4 was deconvoluted into Co-Mo oxycarbide (760 K), β-Mo_2C (860 K), pyrolitic carbon (960 K), η-Mo_3C_2 (1060 K), and carbon in the elemental graphitic form (1149 K) according to literature [26–29]. All of the deconvolutions were carried out using mathematical software (OriginPro, Originlab Co.).

XPS was performed to distinguish the chemical states of Mo, Co, C and O on the carbide surface, and was obtained using a Shimadzu ESCA3200 photoelectron spectrometer equipped with Mg Kα radiation (1253.6 eV, 8 kV, 30 mA). A 1-min argon etching was performed prior to the analysis of the catalysts. The binding energy of C 1s (284.6 eV) was taken as the reference to correct the binding energy of the catalysts. The baseline corrections made for the peak fitting were carried out using the Shirley method provided by the Shimadzu spectrometer manufacturer (Kratos). The spectra of XPS Mo 3d of the Co-Mo carbide samples were deconvoluted using an intensity ratio of 2/3 and a splitting of 3.2 eV, and referenced to the data reported by Quincy et al. [30] and Hada et al. [31]: Mo^0 (Mo $3d_{3/2}$ binding energy: 227.7 ± 0.2, fwhm: 1.2 ± 0.2), Mo^{2+} (228.4 ± 0.1, 1.4 ± 0.2), Mo^{3+} (229.2 ± 0.1, 1.5 ± 0.3), Mo^{4+} (230.1, 1.6 ± 0.2), Mo^{5+} (231.6, 1.65 ± 0.2), and Mo^{6+} (233.0, 1.7 ± 0.2). The spectra of Co $2p_{3/2}$ were deconvoluted to [31,32]: Co^0 (binding energy: 777.6 ± 0.8 eV, fwhm: 1.3 ± 0.1 eV), Co^{2+} (779.9 ± 0.4 eV, 4.2 eV), Co^{3+} (781.6 ± 0.3 eV, 4.7 ± 0.1 eV), and Co^{2+} satellite (786.1 ± 0.3, 5.0 eV). The binding energy of C 1s and O 1s were measured at 282.5–292.0 (for the carbidic and graphitic carbons) and 523–543 eV, respectively. The atomic ratios were determined by the fraction of the divided signal area of a substance to the sensitivity factors of the ESCA 3200.

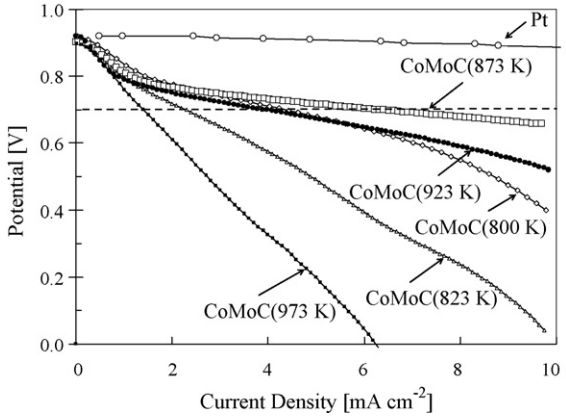

Fig. 1. The *I–V* curves of KC supported Co-Mo catalysts carburized at various temperatures and a 20 wt% Pt/C (not iR corrected). Cell operating conditions: cell temperature, 338 K; reactant gasses, humidified at 353 K without back pressure. Catalyst loadings: anode, 1.0 mg-CoMoC cm^{-2}; cathode 1.0 mg-Pt cm^{-2}.

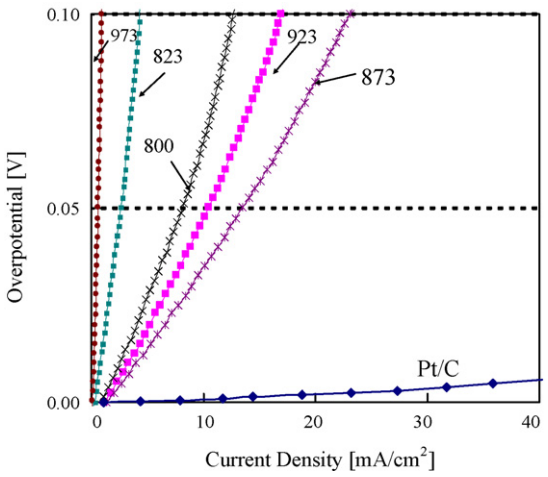

Fig. 2. Anode polarization of the Co-Mo catalyst carburized at various temperatures as a function of current density (not iR corrected). Cell operating conditions: cell temperature, 338 K; reactant gasses, humidified at 353 K without back pressure. Catalyst loadings: anode, 1.0 mg-CoMoC cm^{-2}; cathode 1.0 mg-Pt cm^{-2}.

3. Results and discussion

3.1. Electrocatalytic activity for H_2 oxidation

The *I–V* curves of the KC supported Co-Mo carburized at 800, 823, 873, 923 and 973 K and Pt in the single-stack fuel cell at the anode are shown in Fig. 1 and summarized in Table 1. The open circuit voltages ranged between 0.90 and 0.92 V for the carbides and Pt catalyst. Assuming that the cathodes behave the same, the high OCV observed for the carbides showed a rapid reaction at equilibrium. Among the carburized catalysts, the CoMoC-873/KC displayed the highest performance with an $I_{0.7V}$ of 6.3 mA cm^{-2}. The $I_{0.7V}$ values were in the order of CoMoC-923/KC, CoMoC-800/KC, CoMoC-823/KC and CoMoC-973/KC with the current densities of 3.9, 4.2, 2.3 and 1.4 mA cm^{-2}, respectively. The Pt/C reference showed the high $I_{0.7V}$ of 58 mA cm^{-2}.

Since the *I–V* results mentioned above are the combined activation overpotentials of the anode and cathode, the study was further carried out to elucidate the anode overpotential by measuring the hydrogen oxidation polarization in a two-electrode arrangement. The results of the hydrogen polarization are shown in Fig. 2. The overpotential linearly increases with the current density in the polarization curves over Pt/C, and is in agreement with the literature data [33]. However, the carbides showed a higher overpotential compared to Pt/C that has a slower hydrogen oxidation rate. The CoMoC-873/KC had the lowest polarization, with a voltage loss of 50 mV at 12.4 mA cm^{-2}, followed by CoMoC-923/KC (10.5 mA cm^{-2}), CoMoC-800/KC (8.0), CoMoC-823/KC (2.6) and CoMoC-973/KC (0.6). The results obtained from the overpotential measurements in Fig. 2 illustrated the good relationship between the activity measurements based on the *I–V* curve in Fig. 1. The results also showed that all the in-house prepared MEAs had the same cathodic overpotential.

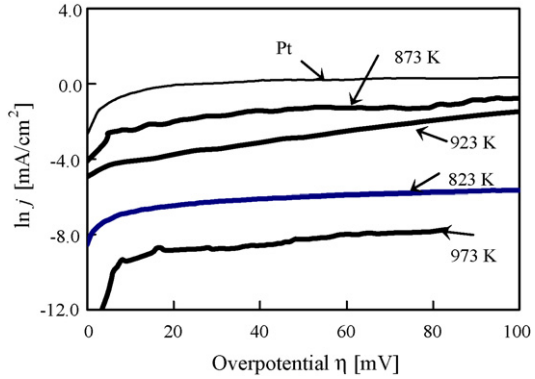

Fig. 3. The slow scan voltammogram (SSV) of Co-Mo carburized at 823, 873, 923 and 973 K. The analyses were carried out in 0.5 M H_2SO_4 at 298 K and a scan speed of 1 mV s^{-1}.

The slow scan voltammetry was measured using a three-electrode cell and the result is shown in Fig. 3. The j_0 for the Pt/C was 1.1 mA cm^{-2}, which was in agreement with that reported by Neyerlin et al. [34] in an acid electrolyte that was between 1 and 50 mA cm^{-2} for the HOR and HER. In this study, the j_0 values for the most active CoMoC-873 was 5.5×10^{-2} mA cm^{-2}, followed by CoMoC-923, -823 and -973, which were 2.0×10^{-3}, 1.9×10^{-3} and 1.0×10^{-4} mA cm^{-2}, respectively. The results obtained from this measurement again showed the agreement of the catalytic activity with the Co-Mo carburization temperature as shown in Fig. 1. Therefore, the catalyst carburization temperature or the degree of carburization should be taken into consideration because of its

Table 1
Performances of Co-Mo catalyst carburized at 800–973 K relative to Pt/C

	Pt/C	Carburization temperature [K]				
		800	823	873	923	973
OCV [V]	0.93	0.92	0.91	0.91	0.92	0.90
$I_{0.7V}$ [mA cm^{-2}]	58	4.2	2.3	6.3	3.9	1.4
$I@\eta_{anode} = 50$ mV [mA cm^{-2}]	203	8.0	2.6	13.5	10.5	0.6
j_0 [mA cm^{-2}]	1.1	n.m.	1.9×10^{-3}	5.5×10^{-2}	2.0×10^{-3}	1.0×10^{-4}
BET surface area [m^2 g^{-1}]	n.m.	n.m.	49	11	1.3	0.4

n.m.: not measured.

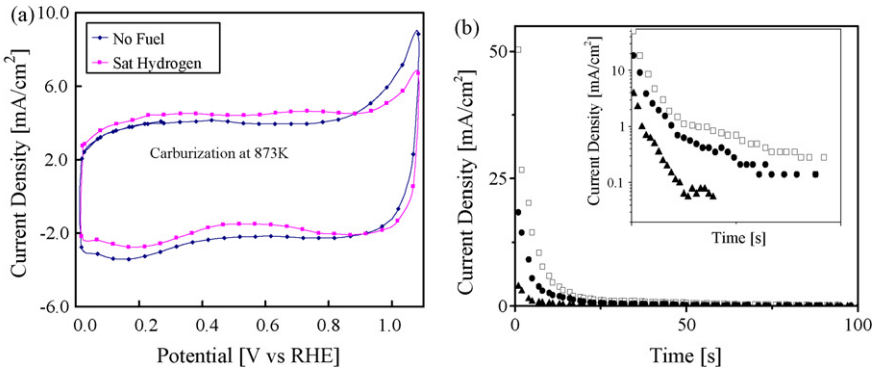

Fig. 4. Voltammetric measurements of carbon supported CoMo carbides in 0.5 M H_2SO_4 at room temperature. (a) CV of CoMoC-873 in a stream of argon and hydrogen, and (b) current/time plots of CoMo carburized at (□) 973, (●) 873 and (▲) 823 K.

significant affect on the catalytic activity during the hydrogen oxidation in a single-stack fuel cell.

3.2. Cyclic voltammetry and passivity in sulfuric acid

The cyclic voltammogram (CV) of the unsupported CoMoC-873 catalyst is presented in Fig. 4a. The CV was measured from 0 to 1.1 V in 0.5 M sulfuric acid with a stream of flowing argon and hydrogen after reaching the steady state. At low potential, no peak corresponding to the redox reaction was observed. On the other hand, at a high potential (above 1 V), the catalyst exhibited a slight increase in current density probably due to corrosion. However, the positive shift of the current density by about 0.5 mA cm^{-2} higher in hydrogen than in argon showed that the catalyst exhibits an activity for the oxidation of hydrogen.

Fig. 4b illustrates the current time plots for the CoMo carburized at CoMoC-823, -873 and -923 K. The experiment gave the direct measure of the corrosion rate of the catalyst in the acidic electrolyte. The CoMoC-823 showed a continuous passivation in sulfuric acid as demonstrated by a rapid falling current. The CoMoC-873 was moderate, while CoMoC-973 demonstrated a poor degree of passivity towards corrosion among the CoMo carbides. A look closer at Fig. 4 (inset) showed that the corrosion current for CoMoC-823 was 63 μA cm^{-2}, followed by CoMoC-873 (140 μA cm^{-2}) and CoMoC-973 (279 μA cm^{-2}). Barnett et al. [10] studied the passivity of the binary carbides of NiW and NiMo to sulfuric acid and reported that the excellent passivity of these carbides are in the range of 20–70 μA cm^{-2}, suggesting the metal oxidation rate of 3–11 pm s^{-1}. The corrosion current of CoMoC-823 was within that range, and is attributed to the high amount of oxides that acts as a corrosion inhibitor. However, CoMoC-873 that exhibited the highest activity despite a relatively high corrosion current was probably due to the presence of carbides that oxidizes upon contact with the acidic electrolyte.

3.3. Performance of Co-Mo carbide catalyst compared to Pt/C

It is of both practical and fundamental interest to compare the catalytic activity of the most active form of the Co-Mo carbide to that of a commercial Pt/C catalyst in which the MEA was prepared in-house and a commercial MEA. Fig. 5 shows the *I–V* characteristics for the single-stack fuel cell prepared using the commercial and in-house MEAs of the 20 wt% Pt/C catalyst. Almost identical performances were obtained for both systems near 0.65 V, but at a higher current density, the in-house MEA performance rapidly dropped. The distinction between the commercial and the in-house MEAs is the catalyst prepared by the binding technique for the former and spray technique for the latter. The spray method probably resulted to an ineffective water management causing a slower water diffusion in the carbon cloth layer, thus increasing the fuel cell resistance. In this study, the preparation of the MEA for the catalysts was carried out in the same manner as the in-house Pt/C catalyst. The current density at the maximum power output, $I@P_{Max}$, obtained from CoMoC-873 was 37 mA cm^{-2}, and was 10.9% versus the in-house Pt/C catalyst MEA (339 mA cm^{-2}). This result is in good agreement with the catalytic performance in Table 1 in which the $I_{0.7V}$ for the CoMoC-873 (6.3 mA cm^{-2}) was also 10.9% of the Pt/C catalyst (58 mA cm^{-2}). Although the carbide electrodes had a performance inferior to the Pt/C electrode, the results exhibit a positive step in the development of low cost Pt-free catalysts.

The durability of the anodes was investigated by the CoMoC-873/KC tolerance towards CO when a stream of CO and H_2 gas was used as the fuel. The concentration of CO in H_2 was varied from 0 to 600 ppm while the anodic overpotential was measured. These results are illustrated in Fig. 6A. The anode overpotential of the Co-Mo carbide catalyst was the lowest in the absence of CO. The overpotential became high (0.09 V) when 50 ppm CO was present. However, when the CO concentration is above 50 ppm, the overpotential change slightly dropped to about 0.01 V for every 100 ppm of CO. The poisoning of the Co-Mo carbide caused by CO up to 50 ppm was probably due to the blocking of the active sites. However, above 50 ppm, the water gas-shift reaction, producing CO_2 and H_2 has likely taken place, resulting in the slower catalyst poisoning. The same measurement over a commercial Pt catalyst is shown in Fig. 6B. The 20% Pt/C catalyst showed that when the CO concentration was increased to 500 ppm, the anode overpotential rapidly

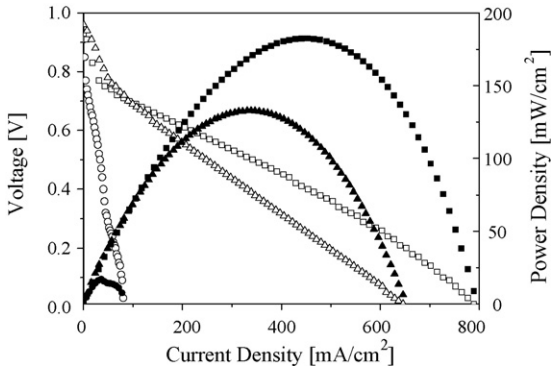

Fig. 5. *I–V* curves of the (□) commercial and (△) in-house 20 wt% Pt/C MEA, with (○) CoMoC-873, and power density curves of (■) commercial and (▲) in-house 20 wt% Pt/C MEA and (●) CoMoC-873 (not iR corrected).

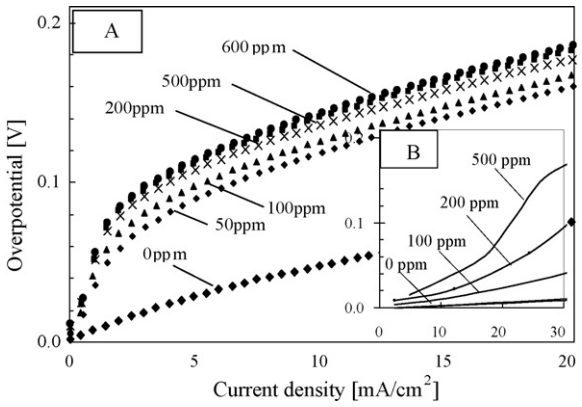

Fig. 6. Anode polarization of (A) KC supported CoMo carburized at 873 K, and (B) Pt/C, in hydrogen mixed with CO gas. The concentration of CO was between 0 and 600 ppm.

increases by about 0.02 V for every 100 ppm due to the blocking of the Pt active site by CO. Based on these results, it can be concluded that the CoMoC-873 has a better durability than Pt catalyst when operating in a high CO concentration.

3.4. Bulk properties of Co-Mo carbides

The XRD spectra for the bulk and KC supported Co-Mo catalysts carburized at 723–973 K are shown in Fig. 7. The XRD spectra showed that the carburization performed at 723, 823 and 873 K resulted in an amorphous-structured catalyst, and when the carburization was carried out above 923 K, the catalyst was found to be more crystalline. This was shown by the low peak intensities of the 723, 823 and 873 K materials and the sharp peaks of the 923 and 973 K carburized catalysts. The pattern mainly showed the presence of Co metal, β-Mo_2C and Co-Mo oxycarbide. The high intensities of β-Mo_2C and metallic Co became clear with an increase in the carburizing temperature to 973 K. This indicates that the Co-Mo oxides were fully carburized to form the Co-Mo carbides during carburization in 20% CH_4/H_2. At carburization temperatures above 923 K, the intensity of the Co metal became definitely higher which is due to the separation of the Co-Mo bimetal. The small peaks for the CoMoC-873 observed between $2\theta = 35^\circ$ and 45° (shown inset of Fig. 7) were assigned to the Co-Mo oxycarbide species. The studies by Bouchy et al. [27] and Nagai et al.

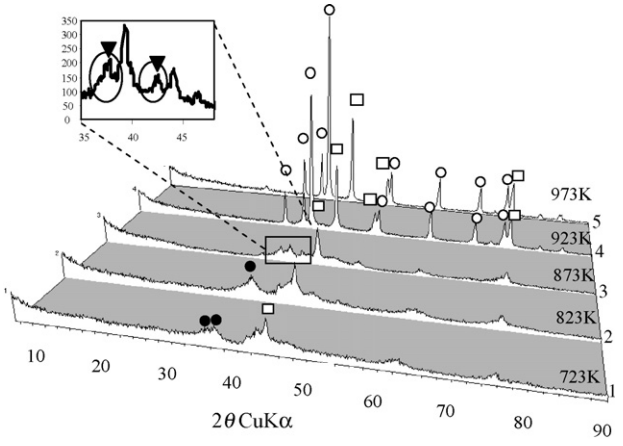

Fig. 7. XRD of Co-Mo carburized at (a) 723 K, (b) 873 K, (c) 873 K, (d) 923 K and (e) 973 K. (▼) Co-Mo oxycarbide, (○) β-Mo_2C, (□) metallic Co and (●) $CoMoO_4$.

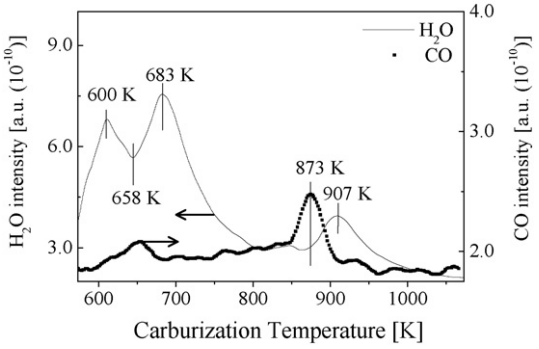

Fig. 8. The evolution of H_2O and CO during temperature programmed carburization of $CoMoO_4$ from 573 to 1173 K in 20% CH_4/H_2.

[21,28] showed by HRTEM that a large amount of the oxycarbide was amorphous, and located on the surface. This is in agreement with the weak diffraction lines observed by XRD for the oxycarbide phase in this study. Since the oxycarbide species were reported to be oxygen deficient on the top sites [35], hydrogen molecules were probably dissociatively adsorbed on the carbon deficient site of the Co-Mo oxycarbide. Ross and Stonehart [36] have indicated that the most active carbide has a carbon deficiency on both the surface and in the bulk, with the carbon deficiency replaced by oxygen.

3.5. Temperature programmed carburization by CH_4/H_2

The evolution behavior of H_2O and CO from the Co-Mo carbide in the stream of 20% CH_4/H_2 during the TPC is shown in Fig. 8. For the evolution of H_2O, two low-temperature peaks centered at 600 and 683 K and a high-temperature peak at 907 K were observed. For the evolution of CO, a small peak was observed at 873 K. In order to examine the transformation of the oxide to the carbide, an XRD analysis was carried out during the carburization at 573, 600, 683, 873 and 907 K. At 600 K, the XRD result showed the presence of Co_3O_4, CoO, MoO_3, MoO_2, $CoMoO_4$, and at 683 K, MoO_2, Mo carbide, CoO, metallic Co were observed. Therefore, as the carburization temperature increased from 573 to 658 K, the reduction of Co_3O_4 to metallic Co and CoO took place. This is evidenced by the XRD analysis shown in Fig. 7 that indicates the presence of metallic Co with low intensities at $2\theta = 44.2^\circ$. As the carburization temperature increased to 683 K, the reduction of MoO_3 to MoO_2 and the reduction of $CoMoO_4$ to the Co-Mo oxycarbide started. The formation of CO at 873 K was related to the complete transformation of $CoMoO_4$ to the Co-Mo oxycarbides since XRD for CoMoC-873 showed a peak intensity for the oxycarbide. Finally, the remaining oxygen from the formation of water centered at 907 K is due to the transformation of the Co-Mo oxycarbides and MoO_2 to β-Mo_2C and metallic Co. This phenomenon verifies the XRD analysis in which the CoMoC-873 illustrated a clear difference in intensity compared to CoMoC-923 that exhibited the sharper peaks of β-Mo_2C and Co metal as shown in Fig. 7. Therefore, based on the TPC measurement, it can be concluded that the principle reactions taking place during the carburization are the reduction of $CoMoO_4$ to Co-Mo by CH_4/H_2, the deposition of carbon by the decomposition of methane, and the dissolution of carbon into the Co-Mo system. Since the activity towards the HOR is the highest for CoMoC-873 and the TPC showed the presence of oxygen at 873 K, the amount of oxygen-containing species (oxycarbide) in the catalyst is one of the factors to take into consideration as the key species. Okamoto et al. [37] in their study on the role of oxygen in tungsten carbide has also shown that the HOR activity was significantly enhanced

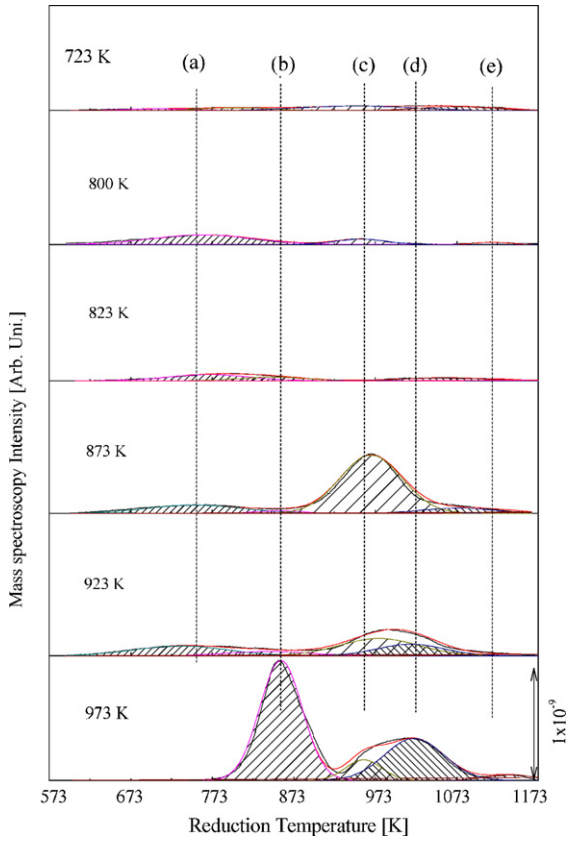

Fig. 9. Formation of CH_4 during TPR performed over Co-Mo carburized at various temperatures. The peaks were deconvoluted into five carbide species and summarized in Table 2. (a) CoMo oxycarbide, (b) β-Mo_2C, (c) pyrolitic carbon, (d) η-Mo_3C_2, and (e) graphitic carbon.

over tungsten carbide that included the most oxygen in the catalyst.

3.6. Temperature programmed reduction by H_2

The TPR profiles of the Co-Mo carbides at various carburization temperatures are shown in Fig. 9. The formation of CH_4 increases with the carburization temperature as shown by the increasing intensity, subsequently indicating the large amount of carbide in the catalyst. The CoMoC-973 exhibited the highest intensity because carburization at high temperature drives the excess surface carbon into the interstitial sites of the catalyst. This shows that the degree of carburization depends on the carburization temperature. The peak for the CH_4 formation centered at 973 K was observed for the CoMoC-873. This peak gradually shifted to 996 and 1020 K for CoMoC-923 and CoMoC-973, respectively. This phenomenon can be attributed to the increase in carbon in the form of graphite. Another CH_4 formation peak that appeared at 860 K for the CoMoC-973 was ascribed to the presence of β-Mo_2C. For the formation of H_2O during the TPR (not shown), the CoMoC-973 catalyst did not show any peak, but was observed for the other Co-Mo catalysts carburized at the lower temperatures. This is in agreement with the TPC that showed no peak of CO and H_2O above 973 K. Therefore, carburization at 973 K can be regarded as fully carburized, and carburization below 973 K can be classified as partially carburized Co-Mo catalyst.

The deconvolution of the CH_4 formation spectra during the TPR is shown in Fig. 9. The intensities were calculated by multiplying the Gaussian curve half width [K] to the peak height [A], both of them

Table 2
Peak areas of CH_4 desorption[a] from five carbon species during TPR for the Co-Mo carbides prepared by various carburization temperatures

Carburization temperature [K]	Co-Mo oxycarbide	β-Mo_2C	PC[b]	η-Mo_3C_2	GC[c]
723	0.18	0.28	0.77	0.42	0.03
800	1.25	0.03	0.35	0.01	0.10
823	0.62	0.30	0.02	0.31	0.04
873	1.01	0.15	4.66	0.48	0.09
923	1.09	0.41	1.62	0.91	0.13
973	0	6.94	1.01	3.39	0.32

[a] Unit: a.u. × 10^{-9} K A (half-width of Gaussian curve [K] × peak height [A]).
[b] Pyrolytic carbon.
[c] Graphitic carbon.

shown in Fig. 9, and are summarized in Table 2. The CH_4 formation was observed at 760 K for all the catalysts except for CoMoC-973. This clearly showed the absence of oxygen (oxycarbide) in the catalyst when carburized at 973 K, and is in agreement with the XRD and TPC measurements. CoMoC-873 showed the highest CH_4 formation at 760 K, which is ascribed to the significant presence of the Co-Mo oxycarbide. The formation of methane at 860 K was attributed to the large amount of β-Mo_2C for CoMoC-973, but was in the small amount for the catalysts carburized at the other temperatures. This high amount of β-Mo_2C was also verified by the high intensity at $2\theta = 37.9^\circ$ by XRD in Fig. 7. Pyrolitic carbons centered at 960 K were observed for CoMoC-873 and -923. The final peak was assigned to the graphitic carbon and was deconvoluted at 1149 K.

The relationship between the intensities of the five carbide species (Table 2) as a function of the catalytic activity (Table 1) is illustrated in Fig. 10. A linear relationship indicated by the solid line was observed for the intensity of the Co-Mo oxycarbide and the activity with a correlation coefficient factor of 0.77. However, no relationship was found between the β-Mo_2C, PC, η-Mo_3C_2 and the activity. On the other hand, graphitic carbon was found to have a negative effect on the activity as shown by the broken line in Fig. 10. This is because graphitic carbon is known to be less active compared to the carbide modified catalyst as reported by Hwu et al. [38]. It has been pointed out that the surface contamination with graphitic carbon (usually known as free carbon) generally produces a decreased activity and is inactive for H_2 oxidation [36]. The presence of the graphitic carbon was found to be accompanied by Mo carbide as illustrated by a high peak for CoMoC-973 at 860 K in Fig. 9 because it is known that the Mo carbide catalyzes the carbon deposition during carburization [17].

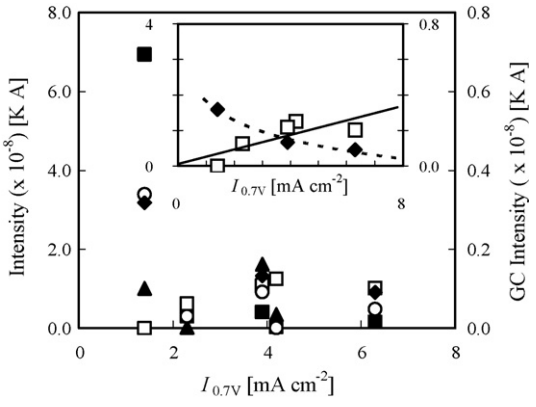

Fig. 10. The intensities of the five carburized species taken from Table 2 as a function of $I_{0.7V}$ from Table 1. (□) CoMo oxycarbide, (■) β-Mo_2C, (▲) pyrolitic carbon, (○) η-Mo_3C_2, and (♦) graphitic carbon.

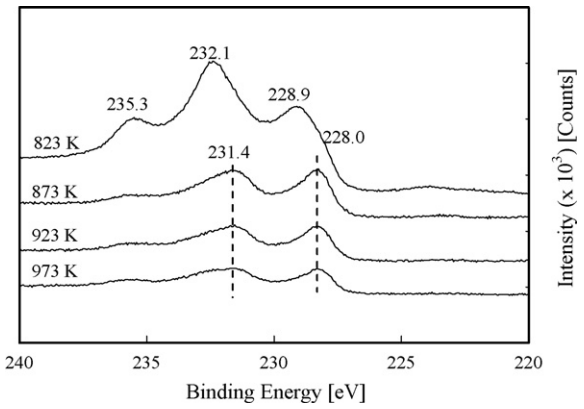

Fig. 11. XPS spectra of Mo 3d of CoMo carbide carburized at 823, 873, 923 and 973 K.

3.7. XPS and surface properties

The XPS measurement was carried out to investigate the surface chemistry involving oxygen that is likely to play a significant role in the HOR. The valence states of atoms on the surface of the carburized catalysts were determined by the deconvolution of the Mo 3d, Co 2p, C 1s, and O 1s envelopes. Fig. 11 illustrates the Mo 3d spectra of the Co-Mo carburized between 823 and 973 K. Three peaks at the binding energies of 235.3, 232.1 and 228.9 eV were observed for the CoMoC-823. However, only two peaks were observed at the binding energies of 231.4 and 228.0 eV when the Co-Mo was carburized above 873 K. The deconvolution of the peaks showed that the average oxidation state dropped from 4.3 to 3.1 when the carburization temperature increased from 823 to 873 K. The dominant species for the CoMoC-823 were Mo^{5+} and Mo^{6+}, contributing 55% of the total surface Mo. While for CoMoC-873, the dominant species were Mo^{2+} and Mo^{3+}, which contributed 57% of the surface Mo. The reduction in the oxidation state showed that the MoO_3 and $CoMoO_4$ were gradually transformed into their respective carbides, in agreement with the result from the TPC and XRD.

Fig. 12 shows the Co 2p spectra of the Co-Mo carburized between 823 and 973 K. The distributions of Co^{2+} for CoMoC-723, -823 and -873 were 66.7, 60.4, and 52.7%, respectively, which showed a decreasing Co valence with the higher carburization temperature. In contrast, the distributions of Co^0 for CoMoC-723, -823 and -923 were 10.8, 11.6 and 33.9%, respectively. These data corresponded to the XRD results in which an increase in the intensity for Co metal was observed between the CoMoC-873 and -923 catalysts. The C 1s spectra of the Co-Mo carburized between 823 and 973 K is shown in Fig. 13. The binding energies for CoMoC-823, -873 and -923 were centered at 285.1 eV while for CoMoC-973, the peak center was 284.9 eV. Since the binding energy for graphitic carbon is reported to be at 284.9 eV [39], carburization at 973 K has resulted in producing a high amount of graphitic carbon on the catalyst surface.

The atomic ratios of O and C to (Co + Mo) for the Co-Mo catalyst carburized between 723 and 973 K are shown in Fig. 14 and Table 3. For the C atomic ratios, the ratio in the oxide precursor and carburization at low temperatures (<823 K) were less than 10. This slight excess of carbon on even the oxide material could be due to the contamination of the samples by prolonged exposure to air, resulting in weakly adsorbed carbonaceous species, and by the process of pressing the powders into the Al substrates for mounting in the spectrometer. However, the C ratio increased to higher than 10 at the higher (>873 K) carburization temperatures. Above 973 K, the C ratio increased to 20. The high C ratio at high temperature is ascribed to the presence of the graphitic carbon which is shown by the TPR results (Fig. 9). On the other hand, the atomic ratios of O

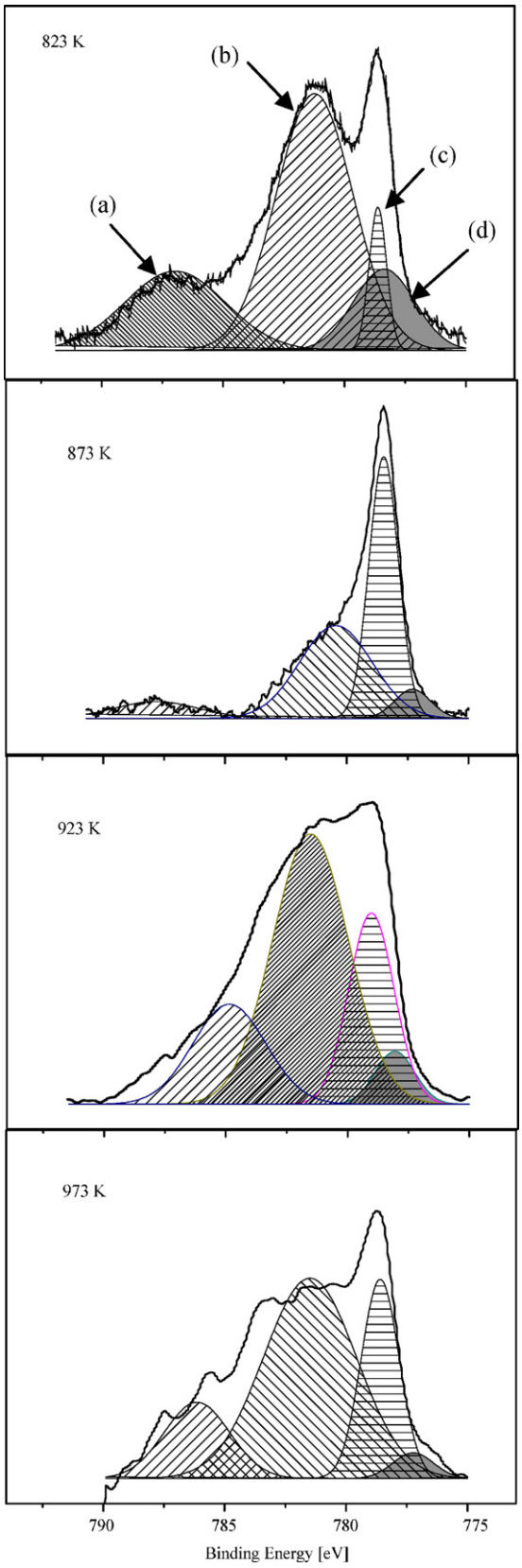

Fig. 12. XPS spectra of Co 2p of CoMo carbide carburized at 823, 873, 923 and 973 K, and were deconvoluted according to (a) Co^0, (b) Co^{2+}, (c) Co^{3+} and (d) satellite Co^{2+}.

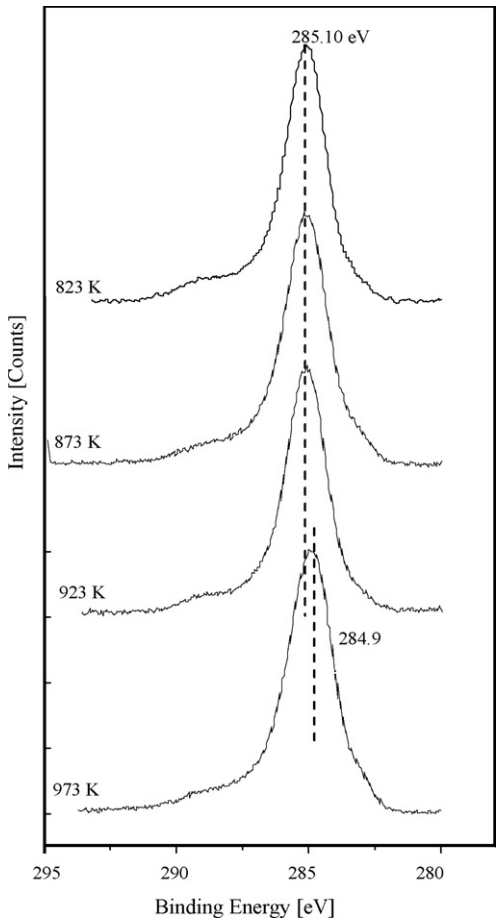

Fig. 13. XPS spectra of C 1s of CoMo carbide carburized at 823, 873, 923 and 973 K.

were observed to be the opposite of the C ratio. At the lower carburization temperatures (<873 K), the O ratio was between 2 and 3, but reached a maximum between 4 and 5 at 873 and 923 K. This high O ratio could be attributed to the O atoms in the lattice spacing diffusing towards the surface as a result of the carburization by the CH_4/H_2 gas. Since the TPR results showed the high presence of Co-Mo oxycarbide and the XPS showed a high O ratio at 873 K, it is concluded that the Co-Mo oxycarbide were the dominant species on the catalyst surface. Finally, at 973 K, the O atomic ratio was nearly zero, which agrees with the TPR and TPC results that showed no formation of water at 973 K.

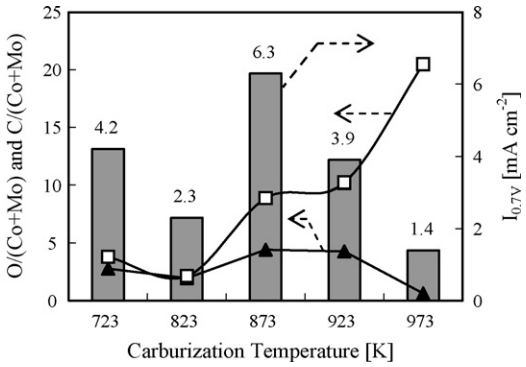

Fig. 14. The atomic ratio of (□) C/(Co + Mo) and (▲) O/(Co + Mo) indicated on the left *Y*-axis and the $I_{0.7V}$ (bar graph) indicated on the right *Y*-axis as a function of the carburization temperature.

Table 3
Atomic ratios of O and C to (Co + Mo) for the catalysts carburized between 723 and 973 K

Carburization temperature [K]	O/(Co + Mo)	C/(Co + Mo)
723	2.76	3.8
823	1.96	2.1
873	4.42	8.9
923	4.27	10.2
973	0.62	20.5

The relation between the $I_{0.7V}$ (Table 1) and the atomic ratios of C and O (Table 3) are illustrated in Fig. 14 (right *Y*-axis). A good relationship can be seen between the atomic ratio of O and the $I_{0.7V}$. However, the carburization at 923 K did not produce the same activity as at 873 K although they have the identical atomic ratios of C and O. This distinction could be related to the bulk properties of the catalyst as shown by the XRD analysis. The CoMoC-873 showed the presence of the Co-Mo oxycarbide and β-Mo_2C in the bulk, while CoMoC-923 mainly consisted of low amounts of oxycarbide and a high amount of β-Mo_2C in the bulk. Kudo et al. [17] in their study to enhance the activity of the W-Mo carbide by a water vapor treatment reported that oxygen in the surface layer does not play an essential role during the catalysis. Furthermore, the TPR result did not show any relationship between the amount of β-Mo_2C and the activity, therefore, the hydrogen electrooxidation is totally contributed by the active Co-Mo oxycarbide.

4. Conclusion

A group of Co-Mo catalysts carburized at various temperatures was prepared. The activity of the partially carburized catalyst (CoMoC-873) resulted in a higher activity for the hydrogen oxidation compared to the perfectly carburized catalyst (CoMoC-973). The performance of the CoMoC-873/KC was found to be the highest at 10.9% versus the Pt/C catalyst in the single-stack fuel cell. The anode polarization obtained from the two-electrode cell showed the low polarization of the CoMoC-873/KC compared to the catalyst carburized at the other temperatures. The measurement by a three-electrode configuration demonstrated the high hydrogen exchange current density, thus showing the high activity of the CoMoC-873/KC. The XRD results showed the presence of the Co-Mo oxycarbide in the bulk which played an important role as the active species for the anodic electrooxidation. The presence of the Co-Mo oxycarbide was further verified by TPC, TPR and XPS. Quantitative analysis of the catalyst by TPR and XPS showed a good relation between the Co-Mo oxycarbide intensity and the activity. These results showed the high potential for not only tungsten carbide, but also cobalt molybdenum carbide as an alternative for the Pt/C catalyst.

Acknowledgement

The authors thank the Scientific Project from NEDO for the financial support.

References

[1] I. Bar-on, R. Kirchain, R. Roth, J. Power Sources 109 (2002) 71.
[2] S.G. Chalk, J.F. Miller, J. Power Sources 159 (2006) 73.
[3] R.B. Levy, M. Boudart, Science 181 (1973) 547.
[4] S.T. Oyama, Catal. Today 15 (1992) 179.
[5] J.G. Chen, Chem. Rev. 96 (1996) 1497.
[6] H.H. Hwu, J.G. Chen, Chem. Rev. 105 (2005) 185.
[7] J.K. Nørskov, T. Bligaard, A. Logadottir, S. Bahn, L.B. Hansen, M. Bollinger, H. Bengaard, B. Hammer, Z. Sljivancanin, M. Mavrikakis, Y. Xuc, S. Dahl, C.J.H. Jacobsen, J. Catal. 209 (2002) 275.

[8] P. Liu, J.A. Rodriguez, Catal. Lett. 91 (2003) 247.
[9] P.N. Ross Jr., J. MacDonald, P. Stonehart, J. Electroanal. Chem. 63 (1975) 450.
[10] C.J. Barnett, G.T. Burstein, A.R.J. Kucernak, K.R. Williams, Electrochim. Acta 42 (1997) 2381.
[11] D.R. McIntyre, G.T. Burstein, A. Vossen, J. Power Sources 107 (2002) 67.
[12] E.C. Weigert, J. South, S.A. Rykov, J.G. Chen, Catal. Today 99 (2005) 285.
[13] G. Bronoel, E. Museux, G. Leclercq, L. Leclercq, N. Tassin, Electrochim. Acta 36 (1991) 1543.
[14] T. Matsumoto, Y. Nagashima, T. Yamazaki, J. Nakamura, Electrochem. Solid State 9 (2006) A160.
[15] K. Lee, A. Ishihara, S. Mitsushima, N. Kamiya, K. Ota, Electrochim. Acta 49 (2004) 3479.
[16] T. Kudo, G. Kawamura, H. Okamoto, J. Electrochem. Soc. 130 (1983) 1491.
[17] T. Kudo, A. Ishikawa, G. Kawamura, H. Okamoto, J. Electrochem. Soc. 132 (1985) 1814.
[18] S. Izhar, S. Otsuka, M. Nagai, J. New Mater. Electrochem. Syst. 11 (2008) 15.
[19] M. Nagai, M. Yoshida, H. Tominaga, Electrochim. Acta 52 (2007) 5430.
[20] J.J. Pietron, C. Laberty, K.E. Swider-Lyons, ECS Trans. 3 (2006) 471.
[21] M. Nagai, K. Matsuda, J. Catal. 238 (2006) 489.
[22] H.A. Al-Megren, T. Xiao, S.L. Gonzalez-Cortesa, S.H. Al-Khowaiter, M.L.H. Green, J. Mol. Catal. A 225 (2005) 143.
[23] M. Nagai, Appl. Catal. A-Gen. 322 (2007) 178.
[24] S. Izhar, H. Kanesugi, H. Tominaga, M. Nagai, Appl. Catal. A-Gen. 317 (2007) 82.
[25] Th. Frey, M. Linardi, Electrochim. Acta 50 (2004) 99.
[26] K. Oshikawa, M. Nagai, S. Omi, J. Phys. Chem. B 105 (2001) 9124.
[27] C. Bouchy, C. Pham-Huu, B. Heinrich, C. Chaumont, M.J. Ledoux, J. Catal. 190 (2000) 92.
[28] M. Nagai, K. Oshikawa, T. Kurakami, T. Miyao, S. Omi, J. Catal. 180 (1998) 14.
[29] M.J. Ledoux, C. Pham-Huu, J. Guille, H. Dunlop, J. Catal. 134 (1990) 383.
[30] B.R. Quincy, M. Houalla, A. Proctor, D.M. Hercules, J. Phys. Chem. 94 (1990) 1520.
[31] K. Hada, M. Nagai, S. Omi, J. Phys. Chem. B 104 (2000) 2090.
[32] K. Hada, M. Nagai, S. Omi, J. Phys. Chem. B 105 (2001) 4084.
[33] Y. Si, R. Jiang, J.C. Lin, H.R. Kunz, J.M. Fenton, J. Electrochem. Soc. 151 (2004) A1820.
[34] K.C. Neyerlin, W. Gu, J. Jorne, H.A. Gasteiger, J. Electrochem. Soc. 154 (2007) B631.
[35] N. Liu, S.A. Rykov, J.G. Chen, Surf. Sci. 487 (2001) 107.
[36] P.N. Ross Jr., P. Stonehart, J. Catal. 48 (1977) 42.
[37] H. Okamoto, G. Kawamura, A. Ishikawa, T. Kudo, J. Electrochem. Soc. 134 (1987) 1645.
[38] H.H. Hwu, B. Fruhberger, J.G. Chen, J. Catal. 221 (2004) 170.
[39] D. Wang, J.H. Lunsford, M.P. Rosynek, J. Catal. 169 (1997) 347.